

# Supplementary material of ‘Pore-scale study of CO<sub>2</sub> desublimation and sublimation in a packed bed during cryogenic carbon capture’

Timan Lei<sup>1</sup>, Kai H. Luo<sup>1\*</sup>, Francisco E. Hernández Pérez<sup>2</sup>, Geng Wang<sup>1</sup>, Junyu Yang<sup>1</sup>, Juan Restrepo Cano<sup>2</sup>, Hong G. Im<sup>2</sup>

<sup>1</sup> Department of Mechanical Engineering, University College London, Torrington Place, London WC1E 7JE, UK

<sup>2</sup> CCRC, Physical Science and Engineering, King Abdullah University of Science and Technology, Thuwal 23955-6900, Saudi Arabia

\* Corresponding author: Email address: k.luo@ucl.ac.uk (Kai H. Luo)

## 1 Grid Convergence test

Grid-independence simulations have been conducted for CO<sub>2</sub> desublimation and sublimation in case Base (see Sec.4.1). The computational domain is covered by three different grids (320 × 320, 640 × 640, and 960 × 960). Temporal evolutions of two metrics are calculated and recorded in Fig. S1, namely the volume fraction of captured solid CO<sub>2</sub> ( $\phi_c$ ) and the averaged temperature of active boundaries ( $\bar{T}_a$ ).

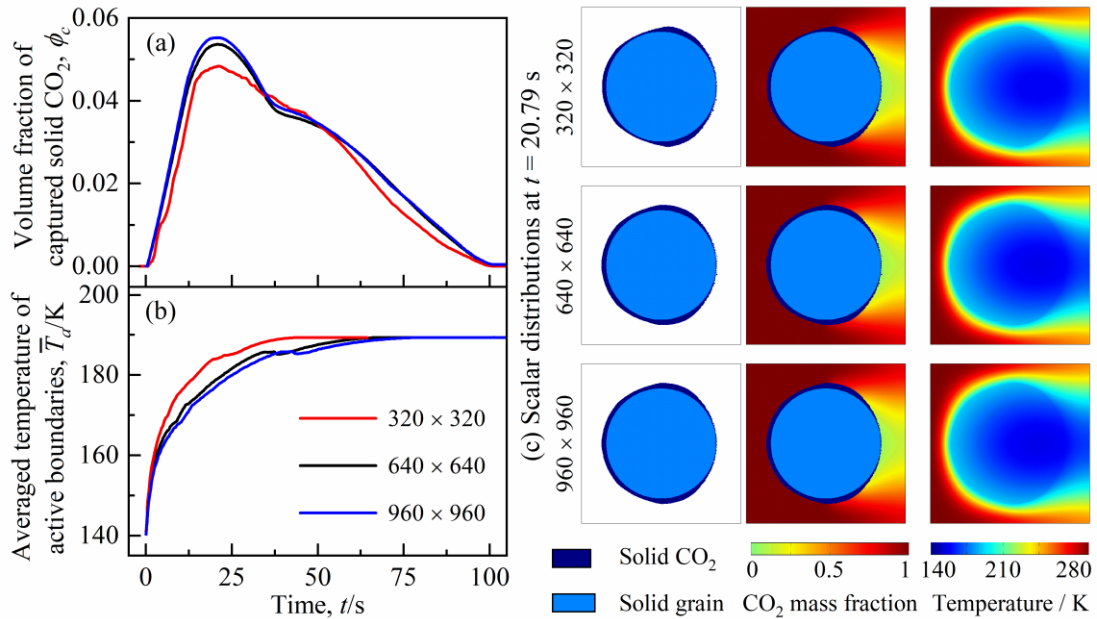


Fig. S1. Grid convergence test. Temporal evolutions of (a) volume fraction of the captured solid CO<sub>2</sub> ( $\phi_c$ ), (b) averaged temperature of active boundaries ( $\bar{T}_a$ ), and (c) contours of solid CO<sub>2</sub>, CO<sub>2</sub> mass fractions, and temperature at the time instant 20.79 s with three grid resolutions in case Base.

By comparing profiles of both  $\phi_c$  and  $\bar{T}_a$ , it is evident that the simulation results for the 640 × 640 and 1024 × 1024 grids exhibit good agreement. The curves for the 384 × 384 coarser grid display a similar pattern to those for the finer grids (i.e.,

640 × 640 and 1024 × 1024), but obvious discrepancies are absorbed between results for the coarser and finer grids. Specifically, the 384 × 384 coarser grid brings about the faster heating of the packing grain ( $\bar{T}_a$ ) and subsequently the lower CO<sub>2</sub> capture performance ( $\phi_c$ ). In addition, the calculated distributions of solid CO<sub>2</sub>, CO<sub>2</sub> mass fraction, and temperature at the time instant 20.79 s are shown in Fig. S1 (c). All these contours under different grid resolutions show a similar pattern, but the captured solid CO<sub>2</sub> for the 384 × 384 coarser grid is observed to be less than those for the other two finer grids (i.e., 640 × 640 and 1024 × 1024). These comparisons suggest that the 640 × 640 grid is sufficiently fine to capture the grid-independent properties CO<sub>2</sub> desublimation and sublimation processes.

## 2 Sensitivity tests of CO<sub>2</sub> mass fraction

This study focuses on evaluating effects of operating conditions, including the initial bed temperature (subcooling degree,  $\Delta T_s$ ), gas feed rate (Peclet number  $Pe$ ), and bed porosity ( $\psi$ ), while maintaining a constant inlet CO<sub>2</sub> mass fraction of  $Y_0 = 1.0$ . To verify the robustness of the present findings, the CO<sub>2</sub> desublimation and sublimation in a cryogenic packed bed are modelled for different CO<sub>2</sub> mass fractions. Through simulations and comparisons for both single-grain and packed-bed cases, the CO<sub>2</sub> capture process is found to exhibit the similar desublimation and sublimation properties as those discussed in Sec. 4. For illustration, results at  $Y_0 = \{0.15, 0.5, 1.0\}$ ,  $\Delta T_s = 0.185$ ,  $Pe = 15.57$  in a packed bed are provided in Fig. S2. That includes temporal evaluations of the captured solid CO<sub>2</sub> ( $v_c$ ), position of the saturation front ( $l_{sat}$ ), and overall mass fraction rate via desublimation and sublimation ( $m_r^*$ ,  $m_{rd}^*$  and  $m_{rs}^*$ ).

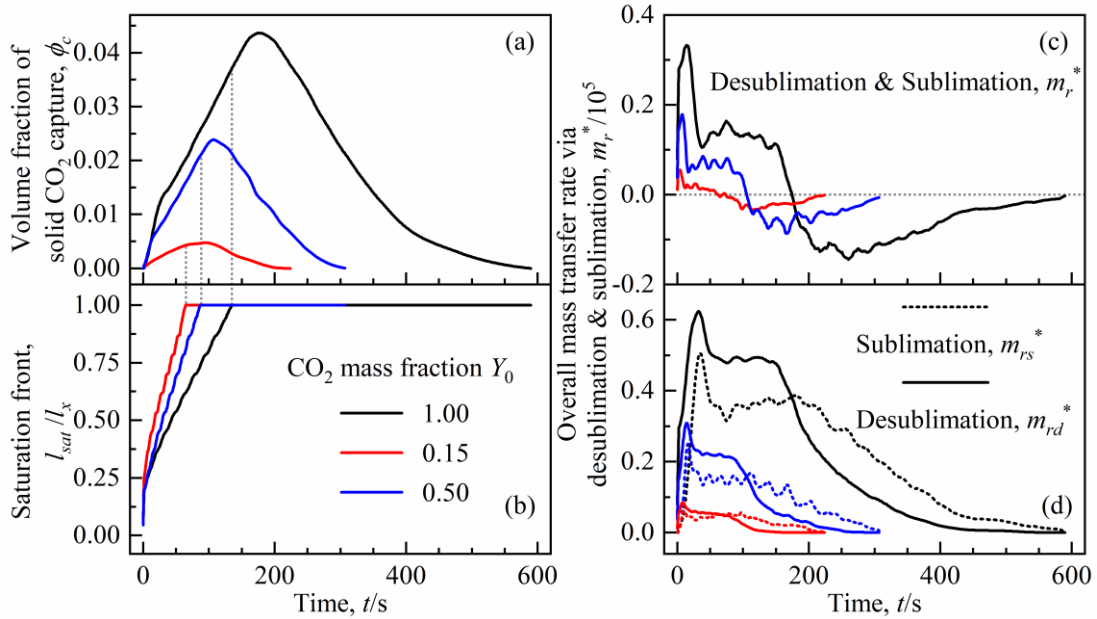


Fig. S2. Effects of CO<sub>2</sub> mass fraction. Temporal evolutions of (a) volume fraction of the captured solid CO<sub>2</sub> ( $\phi_c$ ), (b) position of the saturation front ( $l_{sat}$ ), and (c-d) overall mass transfer rate via desublimation and sublimation ( $m_r^*$ ,  $m_{rd}^*$  and  $m_{rs}^*$ ).

Under each  $Y_0$  value, the desublimation and sublimation processes show a similar tendency. The captured solid  $\text{CO}_2$  ( $\phi_c$ ) exhibits an initial rapid increase followed by a gradual decline toward zero. This behavior is attributed to variations in mass transfer rates ( $m_r^*$ ,  $m_{rd}^*$  and  $m_{rs}^*$ ). Additionally, it is observed that the saturation front ( $l_{sat}$ ) progresses toward the bed outlet as the  $\text{CO}_2$  desublimation proceeds. The saturation time is earlier than the peak point of  $\phi_c$ . In addition to these consistencies with the results in Sec 4.3, the effects of  $Y_0$  are noted. With the increasing  $Y_0$ , the maximum capacity of the packed bed (i.e.,  $\phi_{cm}$ ), the operating time, and the capacity loss decreases. In this study, to efficiently demonstrate the desublimated  $\text{CO}_2$ , the value with the largest  $\text{CO}_2$  capture capacity is selected, namely,  $Y_0 = 1$ .

### 3 Effects of sub-grid surface change

To consider changes in local sub-grid surface, the random pore model is applied to determine the specific surface per unit volume for  $\text{CO}_2$  desublimation and sublimation as [1],

$$a_r = (1 - x)a_{r0}\sqrt{1 - \vartheta\ln(1 - x)}. \quad (\text{S1})$$

Here  $a_{r0}$  is the initial specific surface,  $x$  is the solid  $\text{CO}_2$  conversion rate, and  $\vartheta$  is the structural parameter. Here, we set  $a_{r0} = 1$  and  $\vartheta = 10$  [1]. This calculation equation (S1) gives the maximum surface  $a_r = 1.5a_{r0}$  at  $x = 0.33$ .

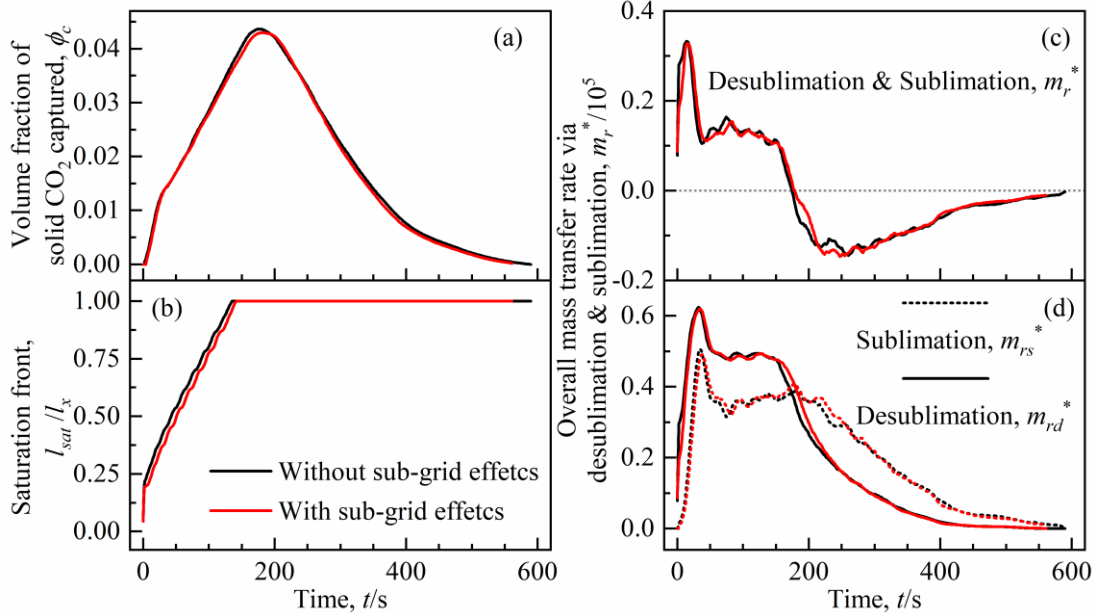


Fig. S3. Sensitivity tests of sub-grid  $\text{CO}_2$  desublimation and sublimation. Temporal evolutions of (a) volume fraction of the captured solid  $\text{CO}_2$  ( $\phi_c$ ), (b) position of the saturation front ( $l_{sat}$ ), and (c-d) overall mass transfer rate via desublimation and sublimation ( $m_r^*$ ,  $m_{rd}^*$  and  $m_{rs}^*$ ).

To demonstrate the significance of including changes in sub-grid surface, the packed-bed test in Sec. 4.3 is simulated again by the present LB model but with  $a_r$

being calculated as in Eq. (S1). The calculated CO<sub>2</sub> desublimation and sublimation properties are recorded versus time in Fig. S3, including volume fraction of the captured solid CO<sub>2</sub> ( $\phi_c$ ), position of the saturation front ( $l_{sat}$ ), and overall mass transfer rate via desublimation and sublimation. For comparison, results of the test without sub-grid effects are included in Fig. S3. From the simulation results, it is obvious that the additionally introduced changes in sub-grid surface have limited impact on the CO<sub>2</sub> desublimation and sublimation properties. This is because, in a packed bed containing multiple grains, the desublimation rate is relatively stronger compared to the supply of CO<sub>2</sub> via the flue gas stream. Furthermore, the change in  $a_r \in [0, 1.5a_{r0}]$  is relatively small. Considering the minimal effects of sub-grid surface change on the desublimation and sublimation of CO<sub>2</sub>, this study uses a constant specific surface as  $a_r = 1$ .

### References

[1] Q. Xu, X. Dai, J. Yang, Z. Liu, L. Shi. Image-based modelling of coke combustion in a multiscale porous medium using a micro-continuum framework, *Journal of Fluid Mechanics* 932 (2022) A51.